Wind Energy

WIND ENERGY
Wind Energ. 2016; **19**:1023–1041
Published online 6 August 2015 in Wiley Online Library (wileyonlinelibrary.com). DOI: 10.1002/we.1880

RESEARCH ARTICLE

Effects of low temperature on the mechanical properties of glass fibre–epoxy composites: static tension, compression, $R = 0.1$ and $R = -1$ fatigue of ±45° laminates

Laurent Cormier[1], Simon Joncas[1] and Rogier P.L. Nijssen[2]

[1] Automated Manufacturing Engineering Department, École de technologie supérieure, 1100 Notre-Dame Ouest, Montréal, Québec, H3C 1K3, Canada
[2] Knowledge Center Wind Turbine Materials and Constructions (WMC), Kluisgat 5, 1771 MV Wieringerwerf, The Netherlands

ABSTRACT

Effects of cold climate exposure on structures made of composite materials are scarcely documented. As a result, even if exceptional wind conditions prevail in some cold regions, uncertainties related to composite materials durability at low temperatures may hinder development of wind energy projects in those regions. Therefore, as part of the Wind Energy Strategic Network (WESNet) of the Natural Sciences and Engineering Research Council (NSERC) of Canada, efforts were made to evaluate the effects of cold climate exposure on the mechanical properties of glass–epoxy composites. Tensile and compressive quasi-static tests as well as tensile ($R = 0.1$) and fully reversed ($R = -1$) fatigue tests were performed on vacuum-infused $[\pm 45]_{2s}$ glass–epoxy composites at −40°C and 23°C. Results for quasi-static tests show an increase of tensile, compressive and shear strengths and moduli at low temperatures. It is also demonstrated that for the stress range under scrutiny, fatigue performance is improved at −40°C for both the $R = 0.1$ and $R = -1$ loading cases. Moreover, the failure mode for $R = -1$ fatigue changed from compressive failure due to buckling of delaminated plies to tensile failure, suggesting a more efficient use of the material. However, if $R = -1$ fatigue results at low temperature are extrapolated towards the very low stresses that are also part of wind turbine blades fatigue load spectrum, fatigue life may be degraded compared with that at ambient temperature. Finally, evidence of visco-elastic behaviour leading to changes in $s - N$ curve slope parameter are reported.

KEYWORDS
fatigue of composites; strength of composites; cold temperature; glass fibre reinforced composites

Correspondence
Simon Joncas, Automated Manufacturing Engineering Department, École de technologie supérieure, 1100 Notre-Dame Ouest, Montréal, Québec, H3C 1K3, Canada.
E-mail: simon.joncas@etsmtl.ca

Received 4 November 2014; Revised 3 April 2015; Accepted 7 June 2015

1. BACKGROUND

With the increased desire for harvesting resources from the world northernmost regions, questions arise regarding the performance and durability of equipments and structures exposed to the harsh environments prevailing there. Often, very limited information exists for operation under such severe conditions and reliability of equipments may have a major influence on projects costs, even more so considering the remoteness of the sites.

A good example of an industry facing challenges for harvesting resources from the North is the wind energy sector. Some northern regions have shown exceptional wind energy potential,[1] but the financial risks associated with operation of a wind plant in those regions are sometimes very high. This risk is due in part to the uncertainties surrounding wind turbines' reliability and unavailability (e.g. due to shut down in case of weather conditions outside their design envelope or failures). The report from the International Energy Agency Task 19 expert group on wind energy in cold climate provides several examples of the challenges facing the wind energy industry in cold regions.[2]

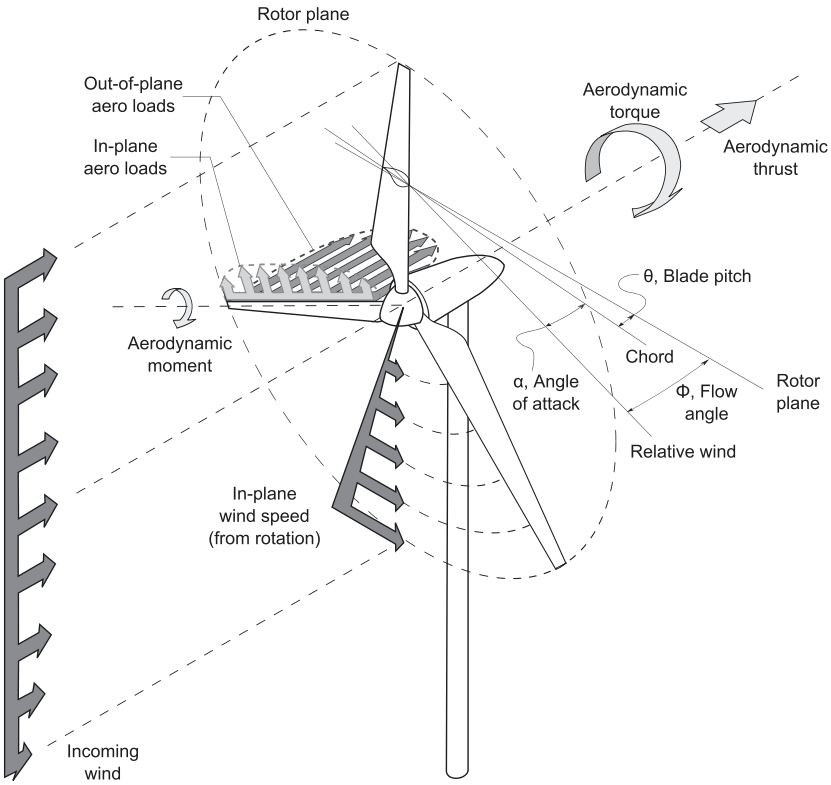

Figure 1. Schematics of simplified aerodynamic loading for a typical utility scale wind turbine.

Among the components that may undergo accelerated failure due to the harsh northern environment, one that could have a major impact on wind plant reliability is the turbine blade. As the blades are some of the most expensive components of utility scale wind turbines,[3] their early failure might have a critical impact on a plant's cost of energy.

In their review of the challenges facing the composite materials industry in civil engineering applications, Kharbari *et al.* suggested that future research on the topic of environmental effects on composites should concentrate on bonded joints and fatigue.[4] More recently, in their review of material degradation in wind turbines, McGowan *et al*. concluded that the main degradation mechanisms of wind turbine blades were fatigue and creep and that a fundamental understanding of these mechanisms still lacked.[5] McGowan also noted that for large wind turbine blades where inertial efforts are important, the exceptionally long fatigue life required – over 10^8 to 10^9 cycles – meant that creep may become the dominant failure mode. In the concluding remarks of this review, the authors state that understanding the implications of service conditions such as moisture and temperature on the fatigue and creep performance of wind turbine blades composites is a necessity.

Figures 1 and 2, respectively, provide a description of typical loads on a utility scale wind turbine and of the geometry and material architecture of wind turbine blades. More detailed descriptions of wind turbine loads or blade structural design can be found in Hau,[6] Brønsted *et al*.,[7] Buckney *et al*.[8] and Griffin.[9]

Figure 1 shows that wind turbine blades are essentially cantilever beams subjected to large flapwise bending aerodynamic loads, coupled to lesser chordwise bending and torsional aerodynamic loads. In addition to the aerodynamic loads depicted in Figure 1, inertial and gravitational loads are present although not illustrated as their value change greatly depending on the blade azimuth and acceleration. It is important to realize that all of these loads vary with time, leading to a very complex fatigue load spectrum. It is also worth noting that for multi-megawatt wind turbines, the gravitational loads and associated edgewise bending may become the structural design driver instead of the aerodynamic loads and flapwise bending.[10]

As shown in Figure 2, the loads result in the blade upper surface being loaded in compression and the lower surface being under tensile stress. It is also seen that unidirectional and ±45° are the two major lamina configurations used in wind turbine blades load bearing structures. It is important to realize that failure of off-axis laminates like ±45° is likely to be dominated by matrix properties. As the latter are notoriously affected by temperature and moisture, it is evident that environmental conditions must also affect the mechanical performance of the composite. The adverse effects of high temperatures have been demonstrated in the past, but little efforts were devoted to identify effects of exposure to low temperatures.

Wind Energ. 2016; **19**:1023–1041 © 2015 John Wiley & Sons, Ltd.
DOI: 10.1002/we

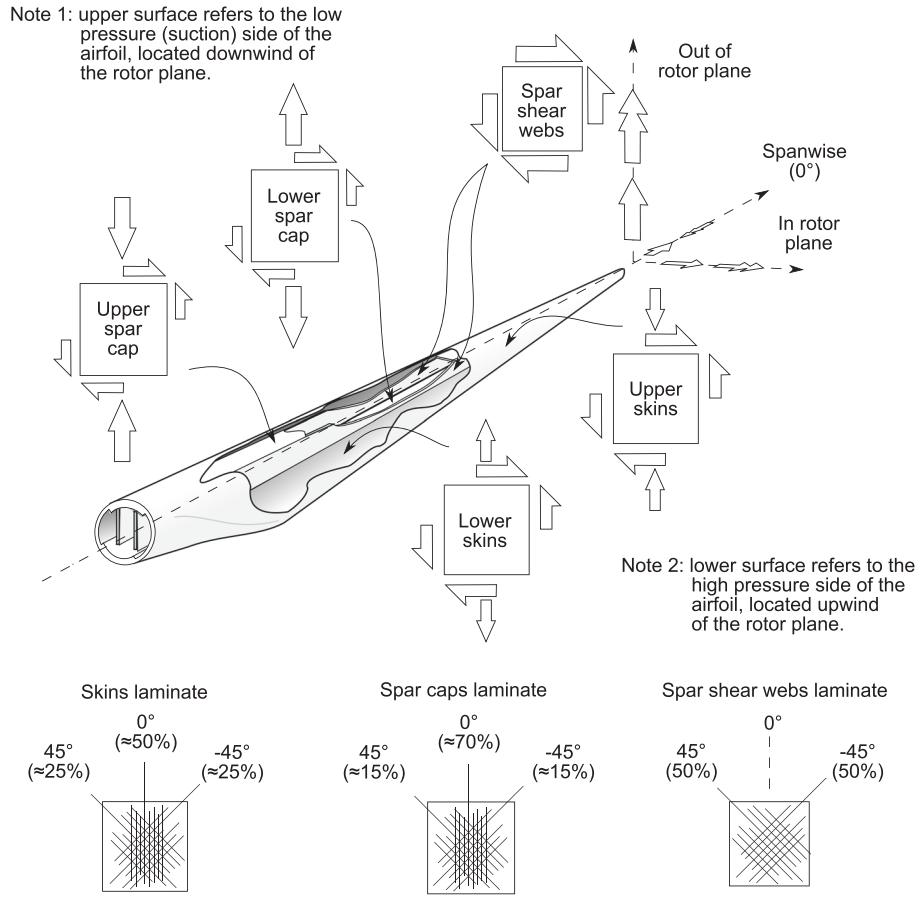

Figure 2. Typical utility scale wind turbine blade materials and loads.

A literature survey by Cormier and Joncas showed an important variability in the conclusions of past research on the effects of low temperature on the static properties of composites.[11] For example, effects of temperature from 200 to 422 K (−73°C to 149°C) on static properties of carbon-reinforced epoxy composites have been studied by Shen and Springer.[12,13] They concluded that low temperatures had little effects on tensile strength and modulus in the fibre direction, but that it could lower the tensile strength of some laminates with off-axis fibres. Bulmanis *et al*. reported reductions of strengths in carbon–epoxy, small reduction of wound glass–epoxy strength and no effects on [0/90] wound glass–epoxy.[14] Dutta also reported results for temperatures ranging between −60°C and 23°C. Low temperature produced compressive strength increase for pultruded glass polyester, no effects on tensile strength of ±45° S_2 glass–epoxy and decreasing tensile strength with increasing 0° fibre content for other S_2 glass–epoxy laminates.[15–17] Cormier and Joncas reported large tensile and interlaminar shear strength increase for unidirectional E glass–epoxy (fibre volume fraction, $v_f \approx 0.55$) at −40°C, but changes in modulus were not significant.[11] A comparable tensile strength increase, as well as an increase in compressive strength, was also reported by Nijssen and Cormier[18] and Cormier *et al*.[19] for another unidirectional glass–epoxy with $v_f \approx 0.48$ tested at −40°C.

Early work on the topic of low temperature fatigue of glass–epoxy composites by Toth *et al*.[20] showed that cryogenic temperatures (20 K, −253°C) led to an increase in static tensile strength and $R = -1$ fatigue lives in triaxial $[-45/0_3/45/0_3/\pm 45/0_3/45/0_3/-45]$ laminates. However, they were unable to quantify the increase in static strength as their test frame was not strong enough to break the cold specimens. Furthermore, all their tests resulted in lives shorter than 100 000 cycles at loads less than 20% of the laminate ultimate tensile stress at 300 K (27°C). Therefore, it is expected that improvements in glass fibre sizing and coupling agents as well as modern resin formulations may lead to modified behaviours. Moreover, the very long life expected from wind turbine blades would require extrapolation of results beyond reason.

A report by Sys also provides some $R = 0.1$ and $R = -1$ fatigue test data on ±10° glass-unsaturated polyester composite with $v_f = 0.5$ tested at −20°C, 20°C and 50°C.[21] Although very little analysis is provided with the data, results suggest that on a strain basis, the low temperature had little effects on fatigue performance.

Another example of work on low temperature fatigue is found in research from Bureau and Denault.[22] They studied the effect of temperatures ranging from −40°C to 50°C on the $R = 0.1$ flexural fatigue of two composite materials. The first laminate was a 2–2 glass twill-polyester construction, and the second was a biaxial glass fabric–polypropylene stacking. Both laminates were of $v_f = 0.6$. According to their results, when normalized by the static strength at their respective temperatures, stress-life ($s - N$) curves for the glass–polyester were superimposed, while those of the glass–polypropylene matrix composite showed a small improvement in fatigue life.

Tang *et al*.[23,24] also showed that tensile fatigue of pultruded multi-axial E glass–vinyl ester laminates with $v_f = 0.36$ (about 0.24 random mat and 0.12 unidirectional roving in the principal direction) was influenced by temperatures in the range of 4°C to 60°C. They suggested that the slope parameter of their $s - N$ equation would decrease with an increase of temperature (clockwise rotation of the $s - N$ curve). They also suggested that when plotting with stresses normalized by the static strength at the test temperature, the $s - N$ curves would rotate about a point situated at $S = 2S_{ut}/3$ and $N = 1000$ cycles. However, their tests were run at 10 Hz, which is relatively high and might result in hysteretic heating of the specimen and interfere with interpreting the results. Moreover, their lowest test temperature was limited to 4°C.

Work from Nijssen and Cormier, conducted as part of the European Upwind project, also provides some results for tensile and reversed fatigue on unidirectional E glass–epoxy laminates ($v_f \approx 0.48\%$) at varying frequencies and temperatures.[18,19] Their results showed that at low frequencies, a temperature of −40°C has minor negative to negligible impact on both tensile and reversed fatigue performance whereas a temperature of 60°C proved to be very detrimental. The laminate glass transition temperature (T_g) was measured to be around 75°C.

Kujawski and Ellyin have shown that in ±45° glass–epoxy laminates, viscous effects play an important role in the dynamic response of the material.[25] They observed that under cyclic loading, an accumulation of creep-induced strains take place and showed that the test frequency influences the cyclic creep rate. As dynamic thermal mechanical analyses under shear loading by Adams and Singh[26] have shown that epoxy resins and composites undergo a low-temperature transition (around $T = -40$°C) that is associated with a marked increase of loss factor, it is possible that low temperatures have deleterious effects on fatigue performance of ±45° glass–epoxy composites.

Understanding the effects of low temperatures on glass–epoxy composites response to fatigue loading is required to allow for the safe exploitation of the wind energy potential in cold regions. In order to help bridging this knowledge gap, an important material testing campaign was included in the Wind Energy Strategic Network (WESNet) of the Natural Sciences and Engineering Research Council (NSERC) of Canada. This paper presents parts of the results from WESNet on the topic of cold climate durability of composite materials for wind turbines. It focuses on the results of the static tensile and compressive tests results as well as tensile and fully reversed fatigue test campaign on biaxial (±45°) glass–epoxy composites.

2. EXPERIMENTAL

2.1. Material description

Test results presented herein are for glass–epoxy laminates of $[\mp 45]_{2s}$ configuration. The material had a $v_f = 0.47$ with a standard deviation $\sigma = 0.01$ as measured by matrix burn-off on a single specimen of 25 × 25 mm taken from a random location on each of ten different 320 × 300 mm plates manufactured for specimen fabrication. The reinforcements are SAERTEX® multiaxial non-crimp fabrics. Each pair of ∓45° plies were pre-stitched fabrics of 831 g/m^2 total areal weight. Each of these stitched plies were constituted of a layer of 600 TEX E–glass strands oriented at −45° and good for 401 g/m^2 followed by 21 g/m^2 of 68 TEX E–glass strands at 90° and another 401 g/m^2 ply at +45°. These sub-plies were all stitched together with 6 g/m^2 worth of polyethersulfone (PES) thread running in the 0° and 90° directions. The matrix is Momentive Epikote™ MGS RIMR 135 epoxy resin cured with a 20/80 part mixture of Momentive Epikure™ MGS RIMH 134 and MGS RIMH 137 curing agents. Based on the resin manufacturer material data sheet, the cured neat resin's $T_g = 84.7$°C at the onset of the storage modulus drop, as measured by dynamic thermal mechanical analysis.

Laminates were manufactured at the Knowledge Center Wind Turbine Materials and Constructions (WMC) by vacuum-assisted resin transfer moulding between two rigid aluminium plates that are bolted together. In order to provide a good control and repeatability of laminates v_f and thickness, shims were inserted between the mould plates to ensure the predetermined spacing based on the target v_f and the areal weight of the fabric were respected. The tooling and resin were preheated to 30°C prior to infusion. The infusion process was performed at 30°C. After infusion, the temperature was increased to 50°C at a rate of 1°C/min. Temperature was then kept at 50°C for 3 h. After the first temperature dwell period, temperature was raised to 70°C at a rate of 1°C/min where it remained for 10 h. The final cooling phase was uncontrolled. After fibre wetting under vacuum, the curing of the laminate is performed at atmospheric pressure to minimize void volume. Specimens were cut using a water-cooled diamond-coated saw.

Wind Energ. 2016; **19**:1023–1041 © 2015 John Wiley & Sons, Ltd.
DOI: 10.1002/we

2.2. Test methods

Static and fatigue experiments were conducted on servo-hydraulic test frames either at École de technologie supérieure's (ETS) Department of Mechanical Engineering material testing laboratory or at WMC. The air temperature around the specimen, the load and the displacement were monitored during the tests. An environmental chamber with temperature and humidity control was connected to the test chamber through a forced air system. The temperature control was on the environmental chamber, and the temperature setpoint was adjusted so that the test chamber temperature matched the test temperature within ±1°C. In order to ensure that the temperature was uniform within the specimens, they were left at the test temperature for at least 15 min prior to testing. Tests were run at a temperature of −40°C and 23°C. The test was interrupted if the air temperature within the test chamber was outside of a ±5°C margin of the target temperature.

Tensile quasi-static experiments were performed in accordance with ISO 527 for off-axis laminates[27] and ISO 14129 for determination of shear properties.[28] The compression tests are not standardized but the general requirements of ASTM D 3039 and ISO 527 were respected (except for the specimen geometry which is described later). Static test specimens were equipped with at least one longitudinal and one transverse foil-type strain gage with a grid resistance of 120 Ω (ETS) or 350 Ω (WMC) with respective excitation voltages of 2 V and 1 V. Low grid excitation voltages were used in order to minimize grid resistive heating. Tensile and compressive moduli were evaluated between 500 and 2500 $\mu\epsilon$, while the shear chord modulus was evaluated between 1000 and 5000 $\mu\epsilon$. Note that despite the extensive necking often encountered in ±45° laminates, failure stress are provided based on engineering strains, which is based on the nominal specimen cross-sectional area. At least five specimens were tested for each condition. It is important to realize that tensile testing of ±45° laminates allows for the characterization of both the tensile properties of the ±45° laminate as well as the shear properties of its constituent 0° unidirectional ply. However, it does not provide any information on shear performance of ±45° materials. The results, assuming limited constraint from the PES stitching and low amount of transverse fibres are to be seen as a description of the shear behaviour of the UD laminates predominant in the spar caps and of the tensile behaviour of the ±45° laminates which form the major part of the skins and spars.

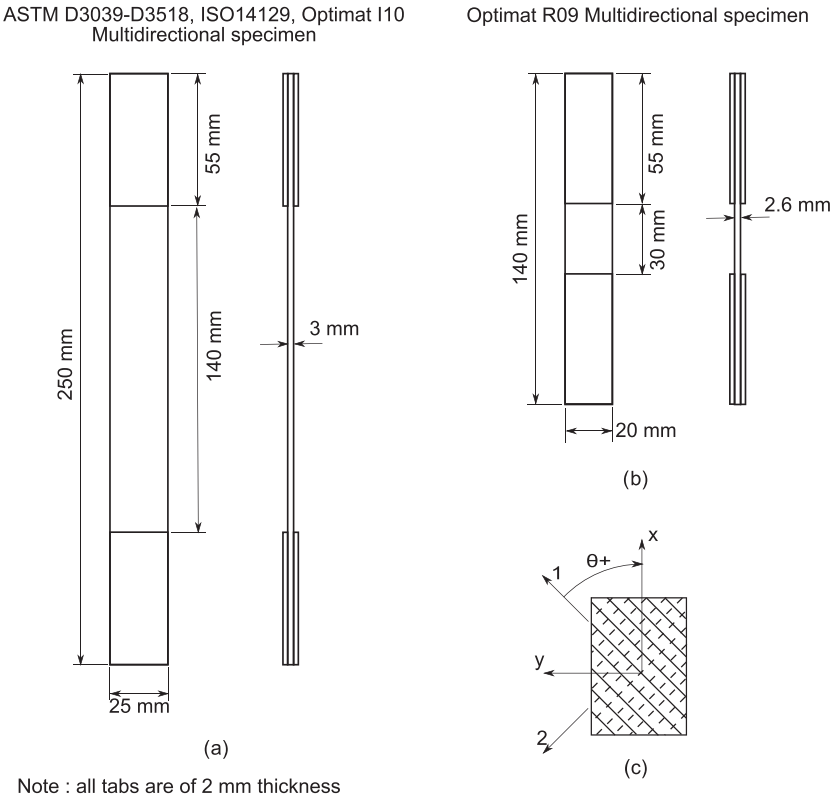

Figure 3. Specimen descriptions : (a) ASTM D3039-D3518, ISO 527-14129, Optimat I10 multidirectional specimen for tension and $R = 0.1$ fatigue tests, (b) Optimat R09 multidirectional specimen for compression and $R = -1$ fatigue tests and (c) specimen and fibre axes convention.

Fatigue experiments were load controlled and performed either at $R = 0.1$ or $R = -1$, with R being defined as the ratio of the minimum stress during the cycle ($s_{\min}$) over the maximum cyclic stress ($s_{\max}$) as per

$$R = \frac{s_{min}}{s_{max}} \tag{1}$$

Therefore, $R = 0.1$ makes for a pure tensile fatigue case and $R = -1$ implies a fully reversed fatigue cycle with an equal tensile and compressive stress magnitude.

Table I. List of fatigue specimens and associated test parameters.

R	Laboratory	Specimen identifier	T	f	$P_{\max}$	A	$s_{\max}$
–	–	–	°C	Hz	N	mm^2	MPa
0.1	ETS	SI02I10	23	3.0	3400	72.9	47
		SU02I10	23	3.0	3825	64.8	59
		TA01I10	23	2.0	4250	64.9	66
		SO07I10	23	2.0	4250	66.8	64
		SU01I10	23	2.0	4250	64.2	66
		SI03I10	23	1.0	5100	73.1	70
		TA03I10	23	1.0	5100	65.7	78
		SR04I10	23	1.4	5950	68.6	87
		SY07i10	−40	2.0	4250	67.7	63
		SR01I10	−40	2.0	4250	66.1	64
		SO08I10	−40	1.4	5100	67.0	76
		SS10I10	−40	1.4	5100	65.0	79
		SY06I10	−40	1.4	5100	68.0	75
		SR05I10	−40	1.0	5950	69.4	86
		SU05I10	−40	1.0	5950	64.6	92
	WMC	SO02I10	23	4.0	4000	67.1	60
		SO03I10	23	4.0	4000	66.4	60
		SU10I10	23	4.0	4000	64.3	62
		SS04I10	23	4.0	4000	65.8	61
		SO04I10	23	2.0	6000	65.9	91
		SU06I10	23	2.0	6000	65.0	92
		SU09I10	23	2.0	6000	64.9	93
		TA08I10	23	2.0	6000	66.9	90
		SY04I10	−40	1.0	6000	67.9	88
		SY05I10	−40	2.0	6000	67.9	88
		SR06I10	−40	2.0	6000	69.4	86
		SR10I10	−40	2.0	5500	69.3	79
		SS03I10	−40	4.0	5250	66.0	80
		SH07I10	−40	4.0	5250	68.4	77
		SR08I10	−40	4.0	4000	69.6	58
		SI08I10	−40	4.0	5000	74.6	67
		SY03I10	−40	4.0	5000	66.1	76
−1	ETS	TB19R09	23	2.0	1750	53.2	33
		SN01R09	23	1.4	2100	52.8	40
		TB12R09	23	1.4	2100	54.1	39
		TB10R09	23	1.0	2450	54.1	45
		SN10R09	23	1.0	2450	53.8	46
		SV07R09	23	1.0	2750	51.7	53
		SN17R09	23	0.8	2800	53.8	52
		TB17R09	−40	1.4	2100	53.6	39
		SN02R09	−40	1.4	2100	53.3	39
		SN03R09	−40	1.0	2450	53.4	46
		SN20R09	−40	1.0	2450	53.9	46
		SV06R09	−40	0.8	2800	51.6	54
		TB03R09	−40	0.8	2800	54.8	51

Wind Energ. 2016; **19**:1023–1041 © 2015 John Wiley & Sons, Ltd.
DOI: 10.1002/we

All $s-N$ curves and their equations are based on the maximum stress $s_{\max}$ or the maximum stress normalized by the static strength at the test temperature s_{max}/S_{ut}. Note that a capital S denotes a strength, while a lower case s is used for stress. In practice, a maximum cyclic load P_{max} was defined, and the stress was calculated according to

$$s_1 = \frac{P}{A} \tag{2}$$

for tension or

$$s_{12} = \frac{P}{2A} \tag{3}$$

for shear. In equations 2 and 3, P is the load and A is the specimen cross-sectional area. The subscripts 1, 2 and 12 (as well as x, y and xy which will be used later) refer to material directions which are defined in Figure 3(c). Since the stress–strain relationship of the laminate is nonlinear and since only a fraction of fatigue specimens were equipped with strain gauges, the analysis is limited to that based on stresses. A sinusoidal waveform was used for the load cycle. Low test frequencies (f) were also used in order to ensure that changes in behaviour at low temperature could not be attributed to a compensation of autogenous (hysteretic) heating.[23,29–32] Moreover, the testing frequency was adjusted as a function of the maximum load in order to maintain an approximately constant strain energy rate as per equation 4 by Krause.[33]

$$f_2 = f_1 \frac{\epsilon_1^2}{\epsilon_2^2} \tag{4}$$

Equation 4 is relative to a reference frequency–strain amplitude, which must be determined experimentally. In the current work, the reference condition was based on surface temperature measurements near the grips at the higher fatigue load level. The acceptable threshold for temperature was set at 35°C before failure. However, average temperatures during tests at room temperature were all below 27°C.

The use of equation 4 for determining test frequencies should make any internal heat generation due to viscous effects uniform over the range of experiments. Moreover, it ensures that if cyclic creep strain build-up occurs, it should also remain similar between experiments at different loads.[25] Table I provides the description of the fatigue test matrix. Each of the $s-N$ curves are obtained from a minimum of six specimens spread over a range of three load levels, allowing for a replication of 50% based on ASTM E 739.[34]

2.3. Specimen description

The tensile specimen geometry is very similar to that of ASTM D3039[35] and ISO 527[27] for multi-axial laminates as well as that of ASTM D3518[36] and ISO 14129[28] for in-plane shear properties of ±45° laminates. This geometry also corresponds to the Optimat I10 specimen geometry.[37] Figure 3(a) provides the general information on the specimen geometry. Note that according to the convention presented in Figure 3(c), the laminate that was used for in this project is $[\mp 45]_{2s}$. However, since in the context of this paper there is no difference between such a laminate and $[\pm 45]_{2s}$, no distinctions will be made from this point on. Although they are not required by the standards, straight tabs made of 2 mm thick ±45° glass–epoxy laminates bonded with epoxy adhesive were used. Tabs were used as, in addition to providing protection against mechanical damage due to gripping, they provide thermal insulation between the grips and the gage section.

Static compression and fully reversed fatigue specimens are of the Optimat R09 geometry. The R09 specimen is a general purpose geometry proposed in the Optimat project. It is a thick, short specimen designed to prevent buckling under compression and has a gage section longer than the specimen width to ensure that off-axis fibres do not run from one tabbed section to the other.[37] A description of the R09 specimen geometry is provided in Figure 3(b).

It is worth noting that some of the materials and specimen peculiarities do not totally comply with the requirements of ISO 14129. First, the presence of stitching and transverse fibres will result in a constraint of the ply pairs reaction to shear. However, since the stitching is non-structural and worth less than 1% of the fibre weight, it is believed that its effect will be limited. Similarly, the presence of 2.5% by weight of transverse glass fibres is expected to have limited effect on the material shear behaviour. Finally, the short length of the compression specimen is also likely to have a somewhat more complex stress distribution than a longer specimen, but the short length is a prerequisite to avoid buckling.

2.4. Determination of $s-N$ parameters

Parameters of the $s-N$ relationship and their statistics are estimated using the maximum likelihood (ML) estimation method. The ML method allows for the proper mathematical treatment of censored data (e.g. runouts or interrupted tests due to time constraints or technical reasons). A detailed description of the ML approach can be found in textbooks such as Nelson's[38] or Gijbels' paper.[39] Applications to the fatigue problems are given in such papers as those from Nelson,[40] Spindel and Haibach[41] and a specific application to fibrous composites is found in Sendeckyj.[42]

Although the application of the ML estimation method is relatively complex, the concept itself is simple. The basic idea is to assume a relationship describing the phenomena being modelled and its underlying statistical distribution. Loosely speaking, the likelihood of a result is the probability of the datum point value being observed (or exceeded in the case of a runout) given the model and the statistical distribution. The likelihood of each data point is then evaluated as a function of the relationship parameters. The total likelihood of the relationship corresponds to the product of the likelihoods of each datum point. The solution of the problem is the set of relationship parameters that maximize the total likelihood and is found by optimization methods. It is interesting to note that the ML approach results in a weighting of the influence of a censored data point on the relationship parameter determination according to how far it lies from the average of the results. On the one hand, the farther a censored point is below the average, the more likely it is (i.e. its probability tends to unity) and the less impact it has on the total likelihood. On the other hand, the farther a data point exceeds the average, the less likely it is (i.e. its probability tends to zero) and the more weight it has.

For the current project, a log–log linear relationship of the $s - N$ curve as that of equation 5 is assumed.

$$\log(N) = \gamma_1 + \gamma_2 \log(s) \tag{5}$$

In equation 5, $\log(s)$ is the base 10 logarithm of the maximum cyclic stress (or normalized cyclic stress) and is the independent variable, $\log(N)$ is the base 10 logarithm of the life in cycles, while γ_1 is the intercept coefficient and γ_2 is the slope coefficient of the relationship. In order to assess the likelihood and as it is desirable that the model provides statistical information like confidence intervals on the $s - N$ curve, an underlying statistical distribution is required. In the present work, it is assumed that the data has a lognormal distribution and that the log-standard deviation σ_L is constant for all stress levels. The ML estimation therefore also has to evaluate a third parameter $\gamma_3 = \sigma_L$. Confidence bounds are given by the approximate normal confidence interval approach. Parameters $\hat{\gamma}_1$, $\hat{\gamma}_2$ and $\hat{\gamma}_3 = \hat{\sigma}_L$ are the estimators that are provided by the ML method as approximate values of the true parameters γ_1, γ_2 and γ_3.

It is worth noting that the determination of confidence bounds by the approximate normal confidence interval approach relies on the asymptotic theory and on the assumption of normal error distribution. However, in the context of fatigue in general, and particularly in part of the present work, a low number of test results preclude the robust verification of those underlying assumptions. Nevertheless, considering that the results of the present work are generally well behaved, the estimations should be acceptable.

3. RESULTS AND DISCUSSION

3.1. Strength and modulus of ±45° laminates

The tensile test on $[\pm 45]_{2s}$ laminates can either be regarded as providing off-axis strength and modulus of the laminate (S_x and E_x) or as an indicator of the shear properties of its cross-ply ($[0/90]_s$) 0° sub-laminate (S_{12} and G_{12}). The following analysis reflects these possibilities, and results are provided for both cases.

3.1.1. Tensile properties.

Results from the tensile experiments on $[\pm 45]_{2s}$ laminates are presented in Table II for both test temperatures. These results show that low temperatures lead to a significant increase of both tensile strength (S_x^+) and modulus (E_x^+) of ±45° laminates. S_x^+ increased by 33% on passing from a temperature of 23°C to a temperature of −40°C, while E_x^+ rose by 20% for the same temperature drop. Inspection of the 95% normal confidence intervals on S_x^+ and E_x^+ shows that the differences in strength and modulus at the two test temperatures are statistically significant, while the change in standard deviation of these properties is not.

These changes are believed to be mostly due to increases in matrix mechanical properties, although the interphase (i.e. the transition region between the fibre surface and the bulk matrix) might also be affected by the temperature change. It appears that internal stresses due to the discrepancy between the matrix and fibre thermal expansion coefficients as well as the interlaminar thermal stress due to the lower temperature do not negatively impact the laminate strength.

Table II. Tensile properties of $[\pm 45]_{2S}$ glass–epoxy.

T	Property	S_x^+	$\sigma_{S_x^+}$	E_x^+	$\sigma_{E_x^+}$
°C	–	MPa	MPa	GPa	GPa
23	Mean	130	4.38	11.8	0.444
	95% bounds	[127, 133]	[3.01, 7.99]	[11.5, 12.1]	[0.306, 0.811]
−40	Mean	173	6.34	14.2	0.861
	95% bounds	[165, 181]	[3.80, 18.31]	[13.2, 15.3]	[0.516, 2.49]

Wind Energ. 2016; **19**:1023–1041 © 2015 John Wiley & Sons, Ltd.
DOI: 10.1002/we

Table III. Shear properties of glass–epoxy 0° sub-plies.

T	Property	S_{12}	$\sigma_{S_{12}}$	G_{12}	$\sigma_{G_{12}}$
°C	–	MPa	MPa	GPa	GPa
23	Mean	65.1	2.20	3.45	0.150
	95% bounds	[63.5, 66.7]	[1.51, 4.01]	[3.34, 3.56]	[0.103, 0.275]
−40	Mean	86.5	3.17	4.38	0.275
	95% bounds	[82.6, 90.5]	[1.90, 9.15]	[4.04, 4.72]	[0.165, 0.795]

Table IV. Compressive properties of $[\pm 45]_{2S}$ glass–epoxy.

T	Property	S_x^-	$\sigma_{S_x^-}$	E_x^-	$\sigma_{E_x^-}$
°C	–	MPa	MPa	GPa	GPa
23	Mean	130	3.43	12.3	0.236
	95% bounds	[126, 134]	[2.14, 8.42]	[12.1, 12.5]	[0.148, 0.580]
−40	Mean	177	7.68	14.6	0.453
	95% bounds	[169, 185]	[4.79, 18.9]	[14.9, 15.0]	[0.283, 1.11]

3.1.2. Shear properties.

Due to the importance of the shear stress component on ±45° laminates under tension loading, the test can also be considered as an indicator of the shear behaviour of UD or cross-ply laminates. Therefore, analysis of the tests from the shear perspective are also provided in Table III.

As expected for matrix-dominated properties, temperature effects are important. As could be anticipated from equations 2 and 3, when measured at a temperature of −40°C, the increase in S_{12} is 33% or the same as for tensile strength. However, the shear chord modulus (G_{12}) rises by 27 % in the same condition, which is more than what was observed for E_x. Again, the 95% normal confidence intervals show the statistical significance of the strength and stiffness increase at −40°C.

3.1.3. Compressive properties.

A summary of results from compression experiments is given in Table IV.

Low temperatures result in a very significant increase of both S_x^- and E_x^- of ±45° laminates. S_x^- increased by 36% on passing from a temperature of 23°C to a temperature of −40°C while E_x^- rose by 24% at low temperature. Based on the confidence intervals, the changes in strength and stiffness are statistically significant to the 5% level.

The fact that S_x^+ and S_x^- are very similar both nominally and at low temperature suggests that the R09 sample geometry was adequate to prevent buckling. It is also worth noting that the stitching may contribute to the good buckling resistance of the specimen as by being stitched in pairs, plies are held together even if delamination occurs.

3.1.4. General considerations on static strength at low temperature.

The current results show a globally improved performance of the $[\pm 45]_{2s}$ laminate at −40°C. These results are in contradiction to earlier work on off-axis composites by Shen and Springer,[12,13] Bulmanis *et al.*[14] and Dutta.[15–17] However, more recent work on unidirectional glass–epoxy by Cormier and Joncas[11] as well as Nijssen and Cormier[18,19] show improvements of mechanical properties at low temperatures. One of the possible causes for this discrepancy is the v_f, which are not stated in the papers from Shen and Springer or Dutta, but that could have a significant effect on low temperature behaviour by influencing the stress distribution around fibres, increasing stress concentration with v_f. The specific thermo-mechanical properties of fibres — e.g. the negative coefficient of thermal expansion (CTE) of carbon fibres — may also have an important effect on thermal stresses occurring at low temperatures.[43] The authors believe that changes in modern coupling agents and matrix formulations might also be involved as improvements to these parameters might allow a shift from a state where mechanical properties were limited by the interphase strength to a state where matrix properties govern failure in more modern laminates.

3.2. $R = 0.1$ Tensile fatigue

A summary of individual specimen results for $R = 0.1$ fatigue tests is provided in Table V.

The ML estimates of the fatigue curves parameters and their respective 95% confidence bounds (based on absolute and normalized stresses) are given in Table VI for both temperatures. The $s - N$ curves based on absolute stresses are provided in Figure 4, while those based on normalized stresses are shown in Figure 5.

Table V. Results for $R = 0.1$ fatigue on $[\pm 45]_{2S}$ glass–epoxy.

Laboratory –	T °C	Specimen identifier –	s_{max} MPa	N^a Cycles
ETS	23	SI02I10	47	+10886752
		SU02I10	59	953283
		TA01I10	66	242181
		SO07I10	64	220179
		SU01I10	66	180607
		SI03I10	70	114619
		TA03I10	78	51655
		SR04I10	87	8824
	−40	SY07i10	63	3867128
		SR01I10	64	+1687988
		SO08I10	76	464906
		SS10I10	79	+79295
		SY06I10	75	752347
		SR05I10	86	258191
		SU05I10	92	70520
WMC	23	SO02I10	60	1670975
		SO03I10	60	1105538
		SO04I10	91	6392
		SS04I10	61	3180623
		SU06I10	92	2624
		SU10I10	62	459045
		SU09I10	93	1956
		TA08I10	90	4931
	−40	SY04I10	88	98133
		SY05I10	88	92502
		SR06I10	86	104809
		SR10I10	79	326375
		SS03I10	80	442294
		SH07I10	77	1047477
		SR08I10	58	+1677069
		SI08I10	67	+2008653
		SY03I10	76	+1004174

[a]Runouts indicated by a '+' sign before the cycle count.

Table VI. Maximum likelihood estimators of $s - N$ parameters for $R = 0.1$ fatigue on $[\pm 45]_{2S}$ glass–epoxy.

Analysis type –	T °C	Property –	$\hat{\gamma}_1$ log(Cycles)	$\hat{\gamma}_2$ log(Cycles) log(MPa)$^{-1}$[a]	$\hat{\gamma}_3 = \hat{\sigma}$ log(Cycles)
Absolute	23	Median	30.0	−13.5	0.215
		95 % bounds	[27.2, 33.0]	[−15.0, −11.9]	[0.146, 0.317]
	−40	Median	27.3	−11.4	0.148
		95 % bounds	[23.8, 31.4]	[−13.4, −9.4]	[0.093, 0.234]
Normalized	23	Median	1.49	−13.5	0.215
		95 % bounds	[1.13, 1.97]	[−15.0, −11.9]	[0.146, 0.317]
	−40	Median	1.73	−11.4	0.148
		95 % bounds	[1.17, 2.57]	[−13.4, −9.4]	[0.093, 0.234]

[a]log(Cycles) for normalized analysis

Wind Energ. 2016; **19**:1023–1041 © 2015 John Wiley & Sons, Ltd.
DOI: 10.1002/we

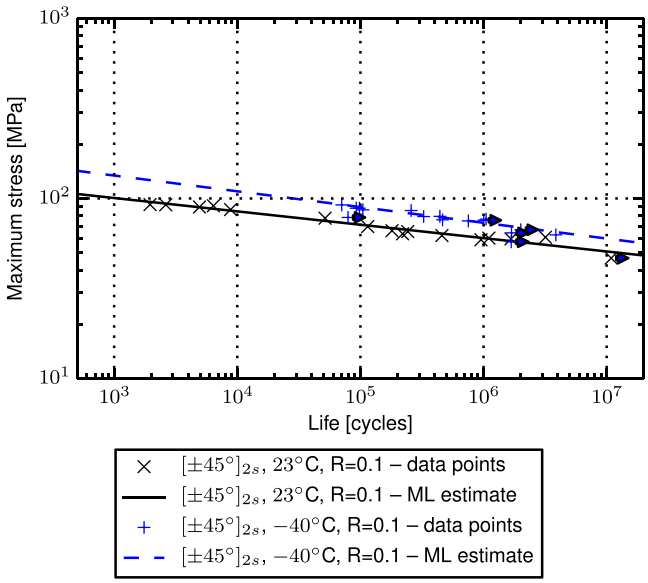

Figure 4. $s-N$ curves for $R = 0.1$ fatigue on $[\pm 45]_{2S}$ glass–epoxy at 23°C and −40°C (solid arrows indicate runouts).

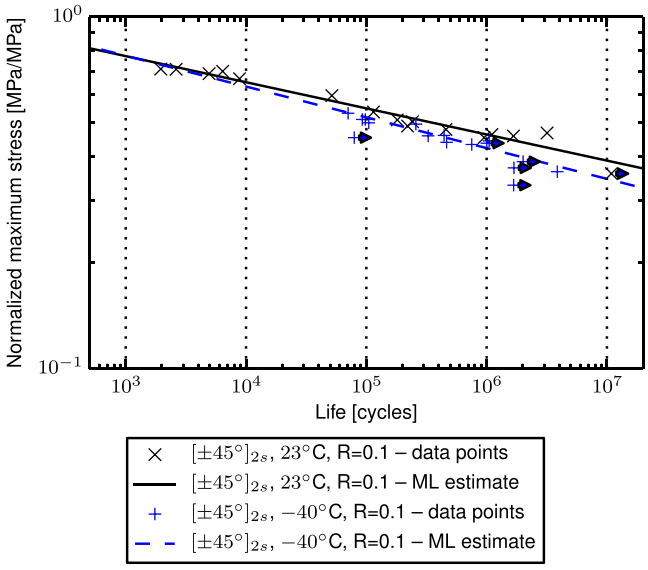

Figure 5. Normalized $s-N$ curves for $R = 0.1$ fatigue on $[\pm 45]_{2S}$ glass–epoxy at 23°C and −40°C (solid arrows indicate runouts).

The following remarks can be formulated based on the results from Table VI and Figure 4.

1. The change in slope of the $s-N$ curves is small but statistically significant (higher slope coefficient at −40°C).
2. The fatigue life at −40°C is improved by more than an order of magnitude compared with that at 23°C.
3. The scatter of the results at low temperature seems to be lower.

The first observation is supported by the fact that although the damage evolution process is somewhat affected, the final failure mode seems to remain unchanged. Figure 6 illustrates the damage evolution for a room temperature test. The damage appears to initiate as matrix cracking between fibres. These cracks then grow along the fibre direction. Aided by the out-of-plane stress near the specimen edges, cracks emanating from each ply eventually coalesce, leading to ply separation near the edges. As these delaminations grow toward the centre of the specimen, the original cracks along the fibres also

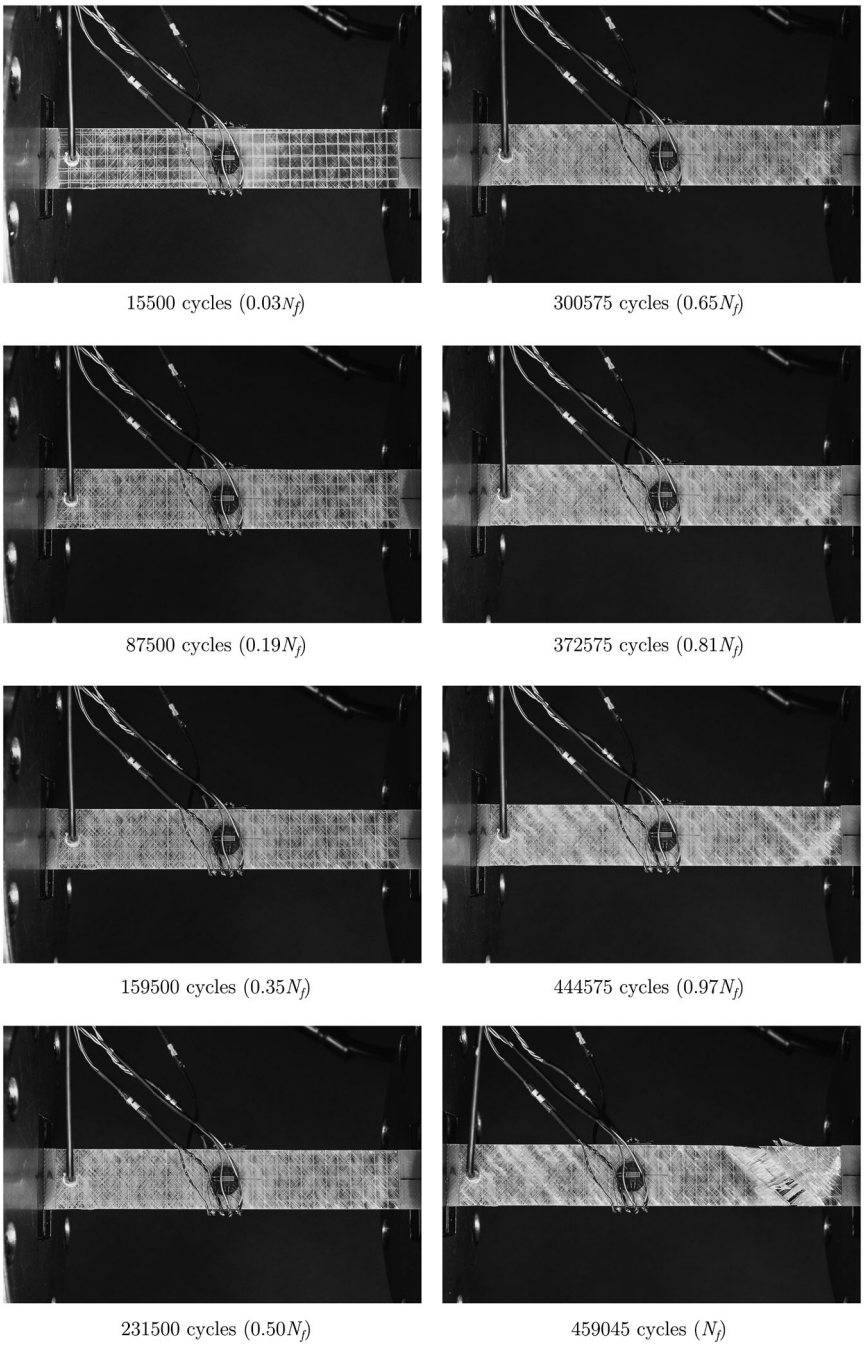

Figure 6. Damage progression for $R = 0.1$ fatigue on $[\pm 45]_{2S}$ glass–epoxy at 23°C (62 MPa, $\approx 0.5S_x^+$).

continue to grow and coalesce, creating additional delaminated regions. These damages continue to grow until final failure of individual plies along their fibre direction.

However, as evidenced by a much lower crack density outside the failure area on tests performed at −40°C, it appears that cracking, coalescence and delamination are delayed substantially at low temperature. In Figure 7, post-mortem photographs of specimens from the two test temperatures after cyclic loading at 4250 and 5950 N show the difference in damage distribution. At room temperature, the failure starts by the development of multiple individual nucleation sites, which interact together to form a broader network of damage, ultimately leading to the specimen failure. In contrast, although cracking along the fibres also initiates randomly over the specimen subjected to low temperature, it seems that there is less

Wind Energ. 2016; **19**:1023–1041 © 2015 John Wiley & Sons, Ltd.
DOI: 10.1002/we

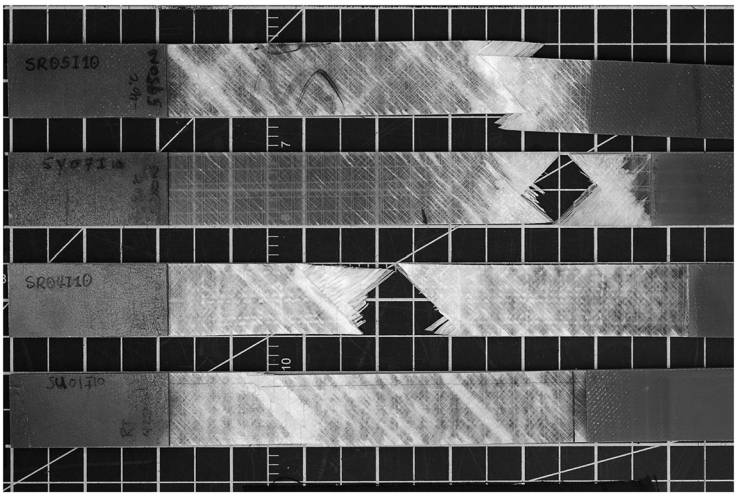

Figure 7. Typical failed $R = 0.1$ fatigue specimens. From top: −40°C, 5950 N (86 MPa); −40°C, 4250 N (63 MPa); 23°C, 5950 N (87 MPa) and 23°C, 4250 N (66 MPa).

interaction between damaged regions. The growth and coalescence phase is thus slowed down and a single region, which probably was initially weaker, collects most of the subsequent damage, leading to a rather localized failure. The reduced interaction between cracks may explain the lower scatter of −40°C fatigue results.

This behaviour can be related to the work of Reifsnider and Case,[44] where effects of matrix properties on failure and failure modes of UD composites were discussed. Their analysis led them to conclude that any temperature change could either provide an improvement or degradation of the composite's strength. This would be due to changes in stress redistribution around broken fibres, and the descriptions of the phenomenon rely on the concept of ineffective length, which represents the distance required for the stress around the break to go back down to the average stress.[44–46] If the matrix is compliant, a large distance is required in order to redistribute the load around the broken fibre, while a stiff matrix can redistribute the load over a smaller distance. Clearly, the latter case results in a higher stress concentration around the break, which further leads to brittle failure. However, in the former case, accelerated failure is also possible because of increased interaction between fibre breaks. Therefore, optimal strength is obtained at an intermediate matrix compliance, and changes of this matrix property due to moisture or temperature may result in either a positive or negative effect on strength. It is proposed here that for a ±45° laminate, a similar process may be active around matrix cracks and interply delaminations and that the stiffening of the matrix may reduce the length over which a stress concentration occurs close to the end of a matrix crack, reducing the potential for crack interactions.

It is believed that the changes in fracture mechanics at low temperature may also follow from a combination of additional factors. First, both the matrix tensile and shear strengths are likely to be improved at low temperature, delaying the apparition of the initial cracks along the fibre direction. Second, changes in matrix and possibly interphase behaviour result in an increase of the interlaminar strength of glass–epoxy composites at low temperature. This was shown by short beam shear test results by Cormier and Joncas.[11] Such an improvement in interlaminar strength would possibly delay the apparition and coalescence of interlaminar cracks that seem to have an important role in the failure process.

The mechanisms described previously appear to override the expected strength reduction resulting from internal tensile stresses developed in the matrix at low temperature as a consequence of the mismatch in fibres and matrix CTE. The micromechanics equations provided by Lord and Dutta[47] and given by equation 6 can be applied to estimate these internal tensile matrix stress due to a change in temperature T and specific moisture content M. In equation 6, the matrix properties, denoted by the subscript m, can be altered according to Chamis' empirical relations of equations 7 and 8 in order to account for the influence of temperature and moisture content.[48] In equation 6, E is the constituent Young's modulus, α is the CTE, β is the moisture swelling coefficient and T_g is the glass transition temperature. F_m is the property reduction factor and can be applied to any matrix property. F_m is simply the ratio of X_m, any given matrix mechanical property, over its reference value X_{m0} and is correlated to the empirical relationship of equation 7. For equations 6–8, subscripts f, w and 0 respectively stand for fibres, wet and reference properties. Finally, in equation 6, the variable $T_{s=0}$ stands for the reference stress-free temperature. $T_{s=0}$ can be assumed to be close to T_g as during curing, chain mobility should allow relatively easy stress relaxation as long as $T \geq T_g$[49] and that sufficient time is given for the visco-elastic relaxation to occur. Note that in the literature, the cure temperature (T_{cure}) has also been reported to be an indicator of $T_{s=0}$.[43] However, in the current context, T_g and T_{cure} are quite close and the definition of $T_{s=0}$ does not influence the reasoning. It should also be noted that since the polymerization reaction is assumed to be complete, the chemical shrinkage is neglected in equation 6.

$$s_{1m}^{T+H} = \frac{E_m E_f v_f}{E_f v_f + E_m(1-v_f)}\left[(\alpha_f - \alpha_m)(T - T_{s=0}) + (\beta_f M_f - \beta_m M_m)\right] \tag{6}$$

$$F_m = \frac{X_m}{X_{m0}} = \left[\frac{T_{gw} - T}{T_{g0} - T_0}\right]^{1/2} \tag{7}$$

$$T_{gw} = (0.005M_m^2 - 0.10M_m + 1)T_{g0} \tag{8}$$

For example, if equation 6 is applied to a UD ply of anhydrous ($M = 0$) glass–epoxy with $v_f = 0.55$ and with E_m varying according to equation 7, the magnitude of matrix thermal stress due to a temperature drop to −40°C is about 20 MPa. Such a stress is quite significant considering that the matrix strength at room temperature is around 70 MPa. Furthermore, as the matrix shrinkage in the direction of each ply principal fibre orientation is restrained, significant interlaminar stresses may be expected. Strengthening processes such as those discussed earlier must therefore be active in order to counteract the negative effects of thermo-mechanical stresses.

Analysis of the normalized results from Figure 5 and Table VI show further evidence of the slope change at low temperature and corroborate the existence of Tang *et al.*[23] 'pivot point' around which the normalized $s - N$ curve rotates for varying temperatures. However, Tang *et al.* located it in the neighbourhood of 1000 cycles and $2S_{ut}/3$, while our results place it somewhat above $2S_{ut}/3$ on the stress axis. This difference might be explained by the higher test frequency in Tang's research leading to increased hysteretic heating and reduced lives at higher stresses. The fact that the normalized $s - N$ curve for −40°C is under that at 23°C in the entire range of stress that was tested also suggests that the mechanisms improving static strength are not as effective in fatigue.

It is also believed that an increased cyclic creep strain build-up associated with a higher loss modulus at −40°C might explain the reduction of the slope parameter and the resulting decrease in fatigue performance on a normalized stress basis. Indeed, Kujawski and Ellyin[25] demonstrated that as a result of the visco-elastic nature of the polymer matrix, cyclic creep strain accumulation contributes to the fatigue failure of ±45° composites. For epoxy and glass–epoxy composites exposed to temperatures in the neighbourhood of −40°C, Adams and Singh reported a peak of loss modulus.[26] As loss modulus is an indicator of the viscous nature of a material, low temperatures should result in increased cyclic creep strain build-up and accelerated failure.

The cyclic creep strain accumulation hypothesis is further corroborated by the consistency of the fatigue results with Kujawski and Ellyin's remark that viscous effects are load dependent. In their work, increasing the test frequency resulted in increased cyclic creep strain rates under high loads while they were reduced at low loads. Put otherwise, an increase in frequency should translate into a counterclockwise rotation of the $s - N$ curve. Accounting for the fact that temperature and frequency can be substituted one to another for determining dynamic properties of polymers,[26] it is possible to draw a parallel between frequency and temperature effects on cyclic creep build-up. However, it is important to realize that although a temperature decrease is usually assimilated to a lesser importance of the viscous behaviour and would normally be assimilated to a frequency increase, Adams and Singh's results suggest otherwise. In fact, it becomes evident that the increased loss modulus at −40°C is equivalent to a frequency reduction. Improved performance at high loads and decreased performance at low loads, such as observed in the present case, are therefore coherent with the assumption of cyclic creep strain build-up.

Finally, as the normalization based on ultimate tensile strength appears to eliminate the shifting of the $s-N$ curve towards the longer lives at low temperature, it is believed that this shift is essentially the result of the matrix strength improvement and reduction in interaction between damage sites. However, the change in slope is not affected by normalization, although the slope difference is visually emphasized on the normalized $s-N$ curve. It is suggested that this change in slope parameter at low temperature might mainly result from increased viscous effects.

3.3. $R = -1$ fully reversed fatigue

Individual results for fatigue at $R = -1$ are provided in Table VII for both 23°C and −40°C. The resulting ML parameters are given in Table VIII. Figures 8 and 9 provide a visualization of the $s - N$ curves, respectively, based on absolute and normalized stresses.

On an absolute basis, the durability of glass–epoxy composites under $R = -1$ loading is strongly affected by a reduction of temperature from 23°C to −40°C. This is evidenced by an improvement in fatigue life of about one decade when compared with room temperature results. However, as opposed to the behaviour at $R = 0.1$, the slope parameter is strongly affected by temperature. This is consistent with the fact that a change in failure mode occurs between 23°C and −40°C.

At room temperature, all specimens failed by ply buckling after extensive delamination, while at −40°C, the load-displacement data indicate that all failures occurred in the tensile loading phase. This suggests that either or both of the following phenomenon occur:

Table VII. Results for $R = -1$ fatigue on $[\pm 45]_{2s}$ glass–epoxy.

T °C	Specimen identifier –	s_{max} MPa	N[a] Cycles
23	SV07R09	53	2888
	TB19R09	33	+2000000
	SN17R09	52	6387
	TB10R09	45	50200
	SN01R09	40	466964
	SN10R09	46	58368
	TB12R09	39	655993
−40	TB17R09	39	3166742
	SN03R09	46	1350723
	SV06R09	54	146550
	SN20R09	46	1385654
	TB03R09	51	364706
	SN02R09	39	2173327

[a]Runouts indicated by a '+' sign before the cycle count.

Table VIII. Maximum likelihood estimators of $s - N$ parameters for $R = -1$ fatigue on $[\pm 45]_{2s}$ glass–epoxy.

Analysis type –	T °C	Property –	$\hat{\gamma_1}$ log(Cycles)	$\hat{\gamma_2}$ log(Cycles) log(MPa)$^{-1}$[a]	$\hat{\gamma_3} = \hat{\sigma}_L$ log(Cycles)
Absolute	23	Median	32.3	−16.7	0.068
		95% bounds	[30.1, 34.7]	[−18.0, −15.3]	[0.032, 0.143]
	−40	Median	19.9	−8.4	0.139
		95 % bounds	[15.5, 25.6]	[−11.4, −5.4]	[0.062, 0.310]
Normalized	23	Median	−2.89	−16.7	0.068
		95 % bounds	[−3.59, −2.33]	[−18.0, −15.3]	[0.032, 0.143]
	−40	Median	1.02	−8.4	0.139
		95 % bounds	[0.18, 5.84]	[−11.4, −5.4]	[0.062, 0.310]

[a]log(Cycles) for normalized analysis

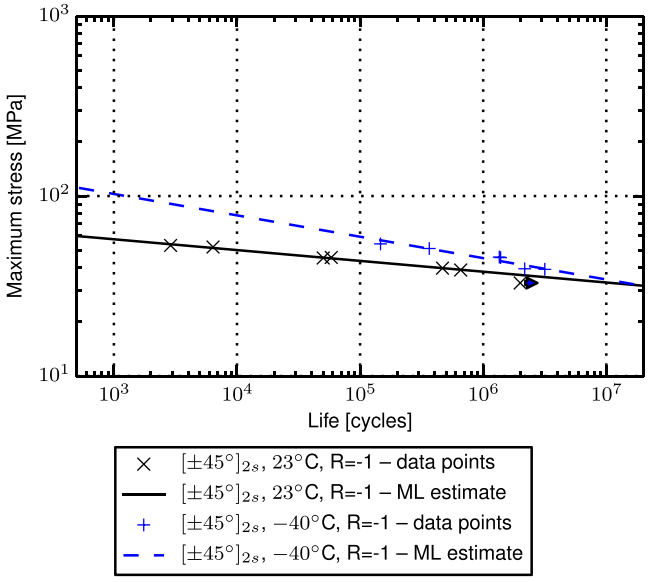

Figure 8. $s - N$ curves for $R = -1$ fatigue on $[\pm 45]_{2s}$ glass–epoxy at 23°C and −40°C (solid arrows indicate runouts).

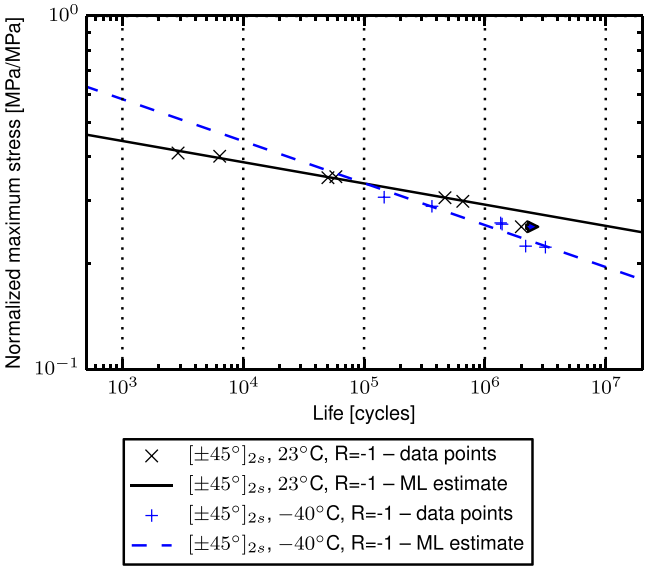

Figure 9. Normalized $s-N$ curves for $R=-1$ fatigue on $[\pm 45]_{2S}$ glass–epoxy at 23°C and −40°C (solid arrows indicate runouts).

1. The ply stiffness rises enough to bring the magnitude of critical buckling stress above that of the stress required to break the matrix.
2. The interlaminar shear strength increases sufficiently to mitigate the delamination growth.

It appears that the mechanisms that lead to the retardation of damage growth and crack coalescence in tensile fatigue are also active in reversed fatigue. However, the added benefit of limited damage during the tensile cycles is that buckling of separated plies is eliminated.

However, even though the failure is tensile for $R=-1$ loading at −40°C, the $R=0.1$ and $R=-1$ fatigue curves are not comparable. The reversed loading specimens fail much earlier and have a higher slope coefficient. This is easily seen by comparing $R=-1$ data in Figure 8 with $R=0.1$ data in Figure 4. Nonetheless, it is interesting to note that moving from a compressive failure due to buckling to a tensile failure is an indicator of more efficient material usage.

Note that although fully reversed fatigue lives are generally increased in the stress range measured in this study, wind turbines are designed for lower stresses and strains required to reach 10^8 to 10^9 cycles. If results are extrapolated to those low stresses, a temperature of −40°C may result in lower lives as a crossover of the $s-N$ curves is visible around 10^7 cycles.

When normalized with respect to the static strength, the improvement in low temperature fatigue resistance is less convincing. Figure 9 shows that for stress above ≈ 35% of S_{ut}, fatigue lives are shorter at −40°C than at 20°C. Therefore, the mechanisms that improve static strength at low temperature appear to be less efficient for fatigue. The fatigue results for $R=-1$ loading are also in agreement with the cyclic creep strain accumulation hypothesis discussed in Section 3.2 as the lives are shortened at low stresses while they are lengthened at higher loads.

4. CONCLUSION

The fatigue performance of glass–epoxy composites at low temperature is of interest for the wind turbine industry because huge wind energy potential exists in northern regions. However, turbine reliability is crucial in these remote regions, and information on the durability of composites in cold climates is scarce. As a result, the WESNet research project included a broad material test program in order to study possible complications or gains related to the use of composites under cold climates, and results for static and fatigue ±45° glass–epoxy are presented.

Results demonstrate that tension and compression strengths and moduli of the $[\pm 45]_{2s}$ laminate as well as the shear strength and modulus of its constituent plies are all significantly improved at low temperature. This is believed to result from increased mechanical properties of the matrix and interphase as well as from the reduced possibility for interaction between damage sites because of increased matrix stiffness. These effects appear to largely outweigh the internal intraply and interply stresses developed because of constrained thermal deformations.

On an absolute stress basis, results for constant amplitude fatigue at $R=0.1$ showed that an approximately tenfold increase in fatigue life can be expected at −40°C when compared with 23°C. Furthermore, the slope parameter was only slightly reduced under those conditions, resulting in improved lives at low stresses. Conversely, the slope parameter of the

Wind Energ. 2016; **19**:1023–1041 © 2015 John Wiley & Sons, Ltd.
DOI: 10.1002/we

$R = -1$ fatigue $s - N$ curve at −40°C is decreased significantly. This reduction of the slope parameter is associated with the transition from compressive failure at 23°C to tensile failure at −40°C. However, this change in slope parameter can result in shorter lives when the $s - N$ curve is extrapolated towards the low stresses required to meet the extended lives expected in wind energy applications.

Nonetheless, when normalized by the static strength at a given temperature fatigue lives of ±45° glass–epoxy composites are shorter in all situations apart for high stresses at $R = -1$, where the change in $s-N$ slope parameter results in improved performance. It is believed that the behaviour exhibited by the normalized stress results is a consequence of the increased cyclic strain build-up because of a loss modulus increase at low temperature.

It was also demonstrated that the damage growth and distribution was affected by low temperatures. At room temperature, strong interactions between initial matrix cracks were observed. This led to multiple zones with comparable levels of damage just before the onset of failure. However, at low temperature, it appears that changes in matrix properties made cracks less likely to coalesce into larger damage, and final failure is more localized.

Therefore, from a practical point of view, it seems that in absolute terms and within the stress ranges studied here, the effects of low temperatures are mainly beneficial for the fatigue durability of ±45° glass–epoxy composites. The main concern remaining for the wind energy industry in regard to the durability of the laminate is with potential degradation of fatigue strength at very low load, which was not studied in the current project but is relevant for the sector. Furthermore, it should be kept in mind that scaling and application to more complex laminates and structures are still scarcely documented in the literature.

ACKNOWLEDGEMENTS

Simon Joncas would like to acknowledge that work reported here was partially carried out with the financial support of the Natural Sciences and Engineering Research Council of Canada (NSERC) as part of the Wind Energy Strategic Network (WESNet). The WESNet is a Pan-Canadian research initiative funded by the industry and the NSERC as a multi-institutional (16 Universities), multi-disciplinary collaborative aiming at the valorisation and expansion of the Canadian wind energy industry.

Laurent Cormier would thankfully acknowledge that the work presented herein was supported through a doctoral grant provided by the NSERC.

Simon Joncas and Laurent Cormier would like to thank The Knowledge Centre Wind turbine Materials and Constructions (http://www.wmc.eu/) for its contribution to the realization of the WESNet test program.

The authors would further like to disclose that while materials were provided free of charge to WMC, the suppliers have had no other implication on the planning, conduct or outcomes of this research.

Natural Sciences and Engineering Research Council of Canada – Wind Energy Strategic Network Project (NETGP 340847-06).

Natural Sciences and Engineering Research Council of Canada (ES D3-379032-2009).

European Commission project Upwind (SES6-CT-2006-019945-UPWIND).

REFERENCES

1. Ait-Idriss B, Pelletier F, Robert L. Étude sur l'évaluation du potentiel éolien, de son prix de revient et des retombées économiques pouvant en découler au québec, *Technical Report R-3526-2004*, 2004.
2. Barig-Gould I, Cattin R, Durstewitz M, Hulkkonen M, Krenn A, Laasko T, Lacroix A, Peltola E, Ronsten G, Tallhaug L, Wallenius T. *Expert group study on recommended practice : wind energy projects in cold climates*, International Energy Agency, 2011.
3. *Renewable energy technology characterizations*, Technical Report TR-109496, U.S. Department of Energy - Office of Utility Technologies, Energy Efficiency and Renewable Energy and Electric Power Research Institute, 1997.
4. Karbhari VM, Chin JW, Hunston D, Benmokrane B, Juska T, Morgan R, Lesko JJ, Sorathia U, Reynaud D. Durability gap analysis for fiber-reinforced polymer composites in civil infrastructure. *Journal of Composites for Construction* 2003; **7**: 238–247.
5. McGowan JG, Hyers RW, Sullivan KL, Manwell JF, Nair SV, McNiff B, Syrett BC. A review of materials degradation in utility scale wind turbines. *Energy Materials* 2007; **2**: 41–64.
6. Hau E. *Wind Turbines: Fundamentals, Technologies, Application, Economics*. Springer-Verlag: Berlin Heidelberg, 2013. DOI: 10.1007/978-3-642-27151-9.
7. Brøndsted P, Lilholt H, Lystrup A. Composite materials for wind power turbine blades. *Annual Review of Materials Research* 2005; **35**: 505–538.

8. Buckney N, Pirrera A, Green SD, Weaver PM. Structural efficiency of a wind turbine blade. *Thin-Walled Structures* 2013; **67**: 144–154.
9. Griffin DA. Windpact turbine design scaling studies technical : area 1 – composite blades for 80 to 120 meter rotor, *Technical Report NREL/SR-500-29492*, National Renewable Energy Laboratory, 2001.
10. Capponi PC, Ashuri T, van Bussel GJ, Kallesøe. A non-linear upscaling approach for wind turbines blades based on stresses. *Proceedings of the Eeuropean Wind Energy Association 2011 Conference And Exhibition*, European Wind Energy Association, Brussels, Belgium, 14–17 March 2011.
11. Cormier L, Joncas S. Effects of cold temperature, moisture and freeze-thaw cycles on the mechanical properties of unidirectional glass fiber-epoxy composites. *51st AIAA / ASME / ASCE / AHS / ASC Structures, Structural Dynamics and Materials Conference*. AIAA-2010-2823, AIAA: Orlando, FL, United States, 2010.
12. Shen CH, Springer GS. Effects of moisture and temperature on the tensile strength of composite materials. *Journal of Composite Materials* 1977; **11**: 2–16.
13. Shen CH, Springer GS. Environmental effects on the elastic moduli of composite materials. *Journal of Composite Materials* 1977: 250–64.
14. Bulmanis VN, Gunyaev GM, Krivonos VV, Mashinskaya GP, Merkulova VM, Milyutin GI, Gerasimov AA, Kuz'min SA. Atmospheric durability of polymer-fiber composites in cold climates. *Mechanics of Composite Materials* 1991; **27**: 698–705.
15. Dutta PK. Structural fiber composite materials for cold regions. *Journal of Cold Regions Engineering* 1988; **2**: 124–134.
16. Dutta PK. Tensile strength of unidirectional fiber composites at low temperatures. *Japan-U.S. Conference on Composite Materials*, Orlando, Florida, USA, 22–24 June 1992; 782–792.
17. Dutta PK. Low-temperature compressive strength of glass-fiber-reinforced polymer composites. *Journal of Offshore Mechanics and Arctic Engineering, Transactions of the ASME* 1994; **116**: 167–172.
18. Nijssen R, Cormier L. Experiments and modelling of influence and interaction of temperature and frequency on fatigue life, *Technical Report Test Report UpWind Deliverable D 3.1.8 / WMC-2010-94*, Knowledge Centre Wind turbine Materials and Constructions, 2011.
19. Cormier L, Nijssen R. Temperature and frequency effects on the fatigue properties of unidirectional glass fiber-epoxy composites. *53rd AIAA / ASME / ASCE / AHS / ASC Structures, Structural Dynamics and Materials Conference*. AIAA-2012-1574, AIAA: Honolulu, HI, United States, 2012.
20. Toth JM, Bailey WJ, Boyce DA. *Fatigue at low temperature*, ASTM STP 857, ASTM international, 1983.
21. Sys W. *Fatigue of materials and components for wind turbine rotor blades* chap. 2, Kensche CW (ed.). EUR 16684 EN, European Commission - Directorate General XIII, Telecommunications, Information Market and Exploitation of Research. Office for Official Publications of the European Communities: Luxembourg, 1996,120–130.
22. Bureau MN, Denault J. Fatigue resistance of continuous glass fiber/polypropylene composites: Temperature dependance. *Polymer Composites* 2004; **25**: 622–629.
23. Tang HC, Nguyen T, Chuang TJ, Chin JW, Wu HF, Lesko J. Temperature effects on fatigue of polymer composites. In *Composites Engineering, 7th Annual International Conference. ICCE/7*. Hui D (ed.). Composites Engineering and College of Engineering, University of New Orleans: Denver, Colorado, 2000; 861–862.
24. Tang HC, Nguyen T, Chuang TJ, Chin JW, Lesko J, Wu HF. Fatigue model for fiber-reinforced polymeric composites. *Journal of Materials in Civil Engineering* 2000; **12**: 97–104.
25. Kujawski D, Ellyin F. Rate/frequency-dependent behaviour of fibreglass/epoxy laminates in tensile and cyclic loading. *Composites* 1995; **26**: 719–723.
26. Adams RD, Singh MM. Low temperature transitions in fibre reinforced polymers. *Composites Part A: Applied Science and Manufacturing* 2001; **32**: 797–814.
27. ISO TC 61/SC 2. ISO 527 - Plastics – determination of tensile properties, Parts 1 to 5, 1993.
28. ISO TC 61/SC 13. ISO 14129 - Fibre-reinforced plastic composites – determination of the in-plane shear stress/shear strain response, including the in-plane shear modulus and strength, by the ±45° tension test method, 1997.
29. Mandell JF, Meier U. Effects of stress ratio, frequency and loading time on the tensile fatigue of glass-reinforced epoxy. In *Long-term behaviour of composites, STP 813*, O'Brien TK (ed.). American Society for Testing Material: Philadelphia, PA, 1983.
30. Hahn HT, Turkgenc O. The effect, of loading parameters on fatigue of composite laminates: Part iv information systems, *Technical Report DOT/FAA/AR-00/48*, U.S. Department of Transportation Federal Aviation Administration Office of Aviation Research, 2000.

31. Kharrazi MR, Sarkani S. Frequency-dependent fatigue damage accumulation in fiber-reinforced plastics. *Journal of Composite Materials* 2001; **35**: 1924–1953.
32. Apinis R. Accceleration of fatigue tests of polymer composite materials by using high-frequency loadings. *Mechanics of Composite Materials* 2004; **40**: 107–118.
33. Krause O. Testing frequency for dynamic tests, *Technical Report OB_TC_N003_DLR*, Deutsches Zentrum für Luft- und Raumfahrt, 2002.
34. ASTM subcommitee E0804. E 739 - standard practice for statistical analysis of linear and linearized stress-life ($S-N$) and strain-life ($\epsilon - N$) fatigue, 2004.
35. ASTM subcommitee D3004. D 3039 - standard test method for tensile properties of polymer matrix composite Materials, 2008.
36. ASTM subcommitee D3004. D 3518 - standard test method for in-plane shear response of polymer matrix composite materials by tensile test of a ±45° laminate, initial adoption 1994 reapproved 2001 and 2007.
37. Nijssen RP. Optidat fatigue of wind turbine materials database, 2011. [Online]. Available: http://www.wmc.eu/optimatblades_optidat.php. (Accessed 24 March 2015).
38. Nelson WB. *Accelerated testing: statistical models, test plans and data analysis*. Wiley Series in Probability and Statistics, Wiley-Interscience, 2004.
39. Gijbels I. Censored data. *Wiley Interdisciplinary Reviews: Computational Statistics* 2010; **2**: 178–188.
40. Nelson W. Fitting of fatigue curves with nonconstant standard deviations to data with runouts. *Journal of Testing and Evaluation* 1984; **12**: 69–77.
41. Spindel J, Haibach E. The method of maximum likelihood applied to the statistical analysis of fatigue data. *International Journal of Fatigue* 1979; **1**: 81–88.
42. Sendeckyj GP. Fitting models to composite materials fatigue data. In *Test Methods and Design Allowables for Fibrous Composites*. ASTM STP 734, Chamis CC (ed.). American Society for Testing and Materials: Philadelphia, PA, 1981; 245–260.
43. White S, Hahn H. Cure cycle optimization for the reduction of processing-induced residual stresses in composite materials. *Journal of Composite Materials* 1993; **27**: 1352–1378.
44. Reifsnider KL, Case S. Mechanics of temperature-driven long-term environmental degradation of polymer based composite systems. *Proceedings of the ASME Material Division: Presented at the 1995 ASME International Mechanical Engineering Congress and Exposition*, Vol. 1. ASME, 1995; 225–230.
45. Gao Z, Reifsnider KL. Micromechanics of tensile strength in composite systems. *Composite Materials: Fatigue and Fracture*, Vol. 4. ASTM, 1993; 453–470.
46. Subramanian S, Reifsnider KL, Stinchcomb WW. Tensile strength of unidirectional composites: the role of efficiency and strength of fiber-matrix interface. *Journal of Composites Technology & Research* 1995; **17**: 289–300.
47. Lord HW, Dutta PK. On the design of polymeric composite structures for cold regions applications. *Journal of Reinforced Plastics and Composites* 1988; **7**: 435–458.
48. Chamis CC. Simplified composite micromechanics equations for hygral, thermal and mechanical properties, *Technical Report NAS 1.15:83320*, NASA Glenn Research Center, 1983.
49. Odegard GM, Bandyopadhyay A. Physical aging of epoxy polymers and their composites. *Journal of Polymer Science Part B: Polymer Physics* 2011; **49**: 1695–1716.